

Demonstration of Sputtering Atomic Layer Augmented Deposition (SALAD): Aluminum Oxide-Copper Dielectric-Metal Nanocomposite

Brian Giraldo, David M. Fryauf, and Nobuhiko P. Kobayashi

Nanostructured Energy Conversion Technology and Research (NECTAR), Department of Electrical and Computer Engineering, Baskin School of Engineering, University of California Santa Cruz, California 95064, United States

Keywords: magnetron, sputtering, atomic layer deposition, ALD, copper, aluminum oxide, optical properties, reflectivity, ellipsometry

Abstract:

Designing a thin film structure often begins with choosing a specific yet conventional film deposition method. In other words, a film deposition system in which two deposition methods complementary one another are physically yet practically hybridized should lead us to new ways of designing thin film structures with structural complexity controlled at a level that has never been envisioned. This premise inspired us to uniquely combine atomic layer deposition (ALD) and magnetron sputtering (SPU) within a single deposition chamber; the combined film deposition system is referred to as sputtering atomic layer augmented deposition (SALAD). SALAD allows us to take full advantages of both ALD's ensuring precise and accurate delivery of precursors and SPU's offering versatility in choosing a chemical element. A SALAD system was designed based on knowledge obtained by computational fluid dynamics with the goal of conceiving a film deposition system that satisfied deposition conditions distinctive for both ALD and SPU, and a prototype SALAD system was assembled by employing off-the-shelf vacuum components. As a demonstration, the SALAD system was utilized to deposit a unique nanocomposite made of a stack of aluminum oxide thin films by ALD and copper thin films by SPU – $\text{AlO}_x\text{-Cu}$ nanocomposite – on a Si substrate. Spectroscopic reflectivity collected on the $\text{AlO}_x\text{-Cu}$ nanocomposite shows unique dispersion features to which conventional effective medium theories used for describing optical properties of composites made of a dielectric host that contains metallic inclusions do not seem to simply apply.

1. Introduction

Searching for answers to questions at the boundary between different disciplines (e.g., magnetism and superconductivity) has repeatedly yielded discoveries of exotic phenomena related to quantum nature of materials. In such exploratory searches, the current approaches focus on uncovering hidden phenomena emerging from materials prepared by rather conventional synthesis techniques, in that, choices of constituent atomic elements set the level of distinctiveness of materials. However, in our view, *engineering* of synthesis techniques is overlooked, and we strongly believe that *engineering* breakthroughs in synthesis techniques will lead us to materials possessing structural complexities that have never been even envisioned, ultimately benefiting *science* of materials–science enabled by engineering. For instance, sputtering (SPU) and atomic layer deposition (ALD) – two prevalent technologies for the deposition of films – have critical shortcomings. While SPU is capable of depositing films using flexible choices from a variety of chemical elements mixed at various compositions, it lacks accurate and precise control on delivering consistent amounts of chemical elements. In contrast, ALD allows depositing films with accurate and precise control on thickness; however, it lacks explicit tunability of chemical composition. These shortcomings become noticeable when a film requires tight thickness control in the range of ~ 0.1 nm and chemical composition that needs to spatially vary with accuracy and precision required for advanced devices. In this paper, we introduce a new concept of hybrid film deposition system, based on SPU and ALD, referred to as Sputtering Atomic Layer Augmented Deposition (SALAD). SALAD brings features not found in conventional stand-alone SPU or ALD, or in easily-imaginable cluster tools built upon SPU and ALD¹, allowing SPU and ALD to operate in a single environment in establishing, for instance, quasi-synchronous processes or sequential processes of the two deposition modes. SALAD allows us to perform "*in-situ*" tuning of surface composition at monolayer level without substantially altering a given thickness, which cannot be done by stand-alone SPU or ALD, or even by a cluster tool if the required total thickness

is large. A multi-layered structure that consists of aluminum oxide and copper – $\text{AlO}_x\text{-Cu}$ nanocomposite – is presented as the demonstration of SALAD.

2. Basic concept of SALAD

Shown schematically in Fig. 1 are the details of a SALAD system consisting of the following three main components: (1) SPU gun, (2) Fast-acting spatial divider (FASD), and (3) precursor inlet/outlet for ALD. As seen in Fig. 1, FASD plays key roles in uniquely establishing a deposition environment suitable for ALD within a deposition chamber optimized for SPU. FASD also minimizes cross-contaminations between ALD and SPU when ALD and SPU run sequentially. FASD is inserted into or retracted from the deposition chamber within a time period of 0.5 s, without breaking the vacuum, to establish a deposition environment

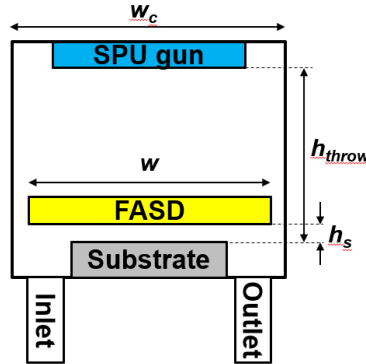


Fig. 1: A prototype SALAD system used for the demonstration is schematically shown, revealing its basic concept. The system is equipped with a sputtering cathode “SPU gun”, a fast-acting spatial divider “FASD”. A substrate is placed underneath FASD. “Inlet” and “Outlet” direct carrier gases and precursors used in ALD. Several dimensional parameters used in the CFD-FEA analysis are also indicated.

suitable for either ALD or SPU, respectively. A SALAD system was designed by carrying out 2D computational fluid dynamics combined with finite-element-analysis (CFD-FEA) to optimize, for instance, the width of FASD w in relation to the chamber width w_c and the throw distance h_{throw} . Table 1 summarizes the key parameters used in the CFD-FEA analysis. Since ALD and SPU co-exist in a single deposition chamber, it is critical to ensure that inserting FASD creates a deposition environment suitable for ALD while h_{throw} is optimized for SPU. For instance, h_{throw} optimized for a specific SPU gun was found to be ~ 60 mm, which was much larger than that normally required for establishing a laminar flow across a substrate in ALD. The use of FASD establishes and maintains a laminar flow that contains ALD precursors over the substrate while h_{throw} is set for optimizing SPU. Fig. 2 shows the distribution of the normalized gas molecule density (ρ) – ALD precursor density – injected into the chamber through the inlet and evacuated via the outlet assuming no reaction occurs over the substrate during ALD (i.e. FASD is inserted) for three different w : (a) 7 mm, (b) 35 mm, and (c) 63 mm. FASD is located at 10 mm above the substrate for all the three

Parameter	Quantity
Chamber width (w_c)	70[mm] (The minimum linear size to accommodate a $\phi 1''$ diameter SPU gun)
SPU throw distance (h_{throw})	$h_{throw} = 10\text{-}120$ [mm] (Variable)
FASD thickness, location (h_s)	2[mm]. $h_s = 10\text{-}30$ [mm] above the substrate
FASD width (w)	$w = 10\text{-}90$ [%] of w_c (Variable)
SPU target width	26[mm]
Heater width	30[mm]
Substrate width	20[mm]
SPU gas type, pressure	Gas type: argon at 300[K], Gas pressure: 1×10^{-3} [Torr]
ALD gas inlet and outlet width	5[mm]
ALD inlet characteristics	Gas type: nitrogen at 300[K], Inlet pressure: 760[Torr], Mass flow: 20[sccm]
ALD outlet characteristics	Outlet pressure: 1×10^{-3} [Torr]

Table 1: Summary of various parameters used in the CFD-FEA analysis.

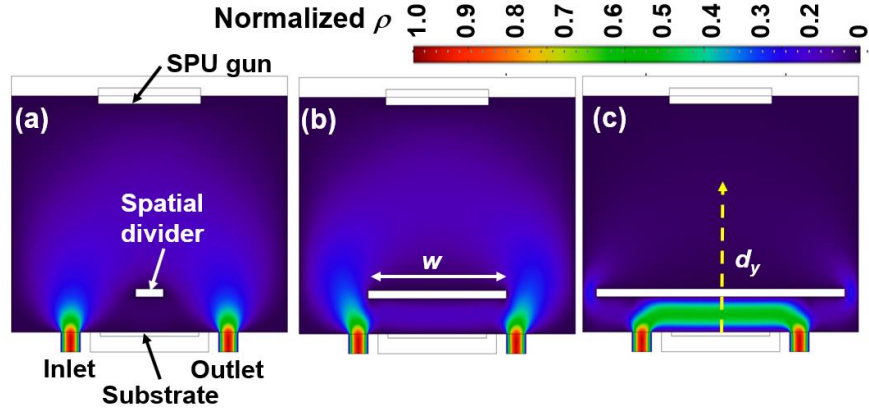


Fig. 2: The gas flow pattern underneath FASD is shown for various w .

cases, suggesting that a laminar flow is established in Fig. 2(c). Fig. 3 shows the dependence of ρ along the yellow dotted line (d_y) shown in Fig. 2(c), indicating the progressive development of a laminar flow as w increases; w needs to be at least 90% of the chamber width for the specific configurations used in the CFD-FEA analysis. Based on our knowledge obtained from conventional SPU using a commercial RF magnetron sputtering system, the deposition rate needs to be in the range of 0.01-0.03 nm/kW/s for various binary/ternary metal oxides, suggesting that the maximum RF power density needs to be in the range of ~ 6 W/cm². Although the CFD-FEA analysis was done on a SALAD system that accommodated a substrate with a diameter of 20 mm as shown in Table 1, all design parameters obtained in the analysis were scaled appropriately in order to assemble a SALAD system that adapted to a substrate with a diameter of 100 mm in the demonstration described below.

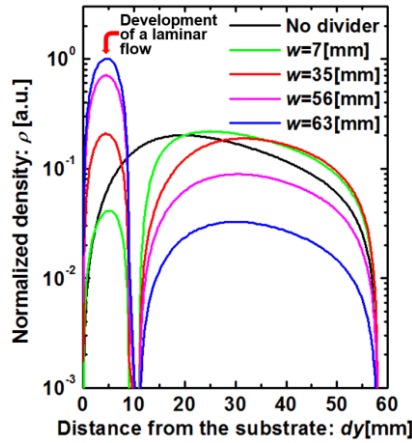


Fig. 3: the dependence of ρ along the yellow dotted line (d_y) shown in Fig. 2(c), indicating the progressive development of a laminar flow as w increases; w needs to be at least 90% of the chamber width for these specific configurations used in the CFD-FEA analysis.

3. Experimental

A prototype SALAD system was built with a SPU gun that accommodated a sputtering target with a diameter of 50 mm. Provided an appropriate h_{throw} , the SALAD system accommodates a substrate with a diameter up to 100 mm. A series of deposition runs were carried out to distinctively demonstrate the capability of the SALAD system intended for unifying ALD and SPU in a single chamber. For the demonstration, a simple multi-layered structure made of aluminum oxide (AlO_x) and copper (Cu) was used; AlO_x and Cu were deposited by ALD (i.e., ALD AlO_x) and SPU (i.e., SPU Cu), respectively. AlO_x was chosen because of the level of its maturity as a dielectric material routinely deposited by ALD while Cu was chosen because of its free-electron density much higher than that of silver^{2,3} and gold^{4,5,6,7} – the two metallic materials commonly used as inclusions embedded in dielectric materials. Aluminum (Al) could be an alternative to Cu; however, Al was avoided as it would form AlO_x when Al was exposed to the AlO_x ALD processes that used oxidizer.

AlO_x resulting from the oxidation of Al deposited by SPU would not be easily distinguished from the AlO_x deposited by ALD. Cu also forms a variety of oxides including Cu_2O , CuO , and Cu_4O_3 that would significantly modify dielectric properties of ALD AlO_x by behaving as a band insulator⁸, a charge transfer insulator⁹, and a mixed-valence compound consisting of Cu_2O and CuO ¹⁰, respectively; however, these oxides can be clearly distinguished from ALD AlO_x in analytical perspectives and are suitable for studying intermediate phases – multi-layered structures consisting of AlO_x and Cu – existing between ALD AlO_x and SPU Cu – referred to as AlO_x -Cu nanocomposite.

Table 2 summarizes ALD and SPU conditions used for depositing the AlO_x -Cu nanocomposite for the demonstration of SALAD. Other deposition parameters during ALD include the pulse duration of trimethylaluminum (TMA) and water (H_2O) being 80 ms and 150 ms, respectively, and the flow rate of the Ar purge gas being 20 sccm. The AlO_x -Cu nanocomposite was deposited by the following sequence: a cycle of ALD was completed to deposit AlO_x and followed by a SPU step with a duration of 3 s, which defined a single SALAD cycle that was repeated for 300 times. In other words, with the deposition parameters provided in Table 2, each of ALD AlO_x and SPU Cu was deposited with the same nominal thickness of 0.13 nm during an ALD cycle and a subsequent SPU duration. All silicon substrates used in the demonstration were directly pulled from their original wafer box and no pre-deposition cleaning procedure was done. Thus, 300 SALAD cycles were expected to yield a AlO_x -Cu nanocomposite with nominal thickness of 78 nm with effective chemical composition of $\text{AlO}_{x0.5}\text{Cu}_{0.5}$ with assumptions that a single SALAD cycle yielded a 0.13 nm thick ALD AlO_x layer followed by a 0.13 nm thick SPU Cu layer with no changes in their respective deposition rates obtained by performing two separate calibration processes and without any intermixing of the two. A FilmTek 4000 spectroscopic reflectometry/ellipsometry (SRE) equipped with a UV-Visible light source was used to obtain spectral reflectivity R from the following samples prepared by the SALAD system: 200 nm thick Cu (i.e., no ALD AlO_x was done), 40 nm AlO_x (i.e., no SPU Cu was done), and the AlO_x -Cu nanocomposite with a nominal thickness of 78 nm. The SRE system acquires absolute R by comparing R of a sample with that obtained from a known reference – in our case a bare silicon wafer covered with natural oxide. All R measurements were done at the light incident angle of 70 degrees with respect to the surface normal of the samples.

SALAD Deposition Parameters			
ALD parameters		SPU parameters	
Precursors	TMA	SPU target	99.999% Cu
	H_2O	DC Power	100 W
Purge gas	Argon	SPU Gas	Argon
Deposition temperature	150 °C	Deposition temperature	150 °C
Base chamber pressure	0.14 Torr	Deposition pressure	0.24 Torr

Table 2: Summary of ALD and SPU conditions used for depositing the AlO_x -Cu nanocomposite.

4. Results and Discussion

Fig.4 shows a time-progressive change in the background pressure in the SALAD system showing four SALAD cycles, out of the total 300 SALAD cycles, sampled during the preparation of the AlO_x -Cu nanocomposite. Each SALAD cycle comprises: a TMA pulse denoted by the red dotted vertical line, a purge for TMA, a H_2O pulse denoted by the green dotted vertical line, a purge for H_2O , and a SPU duration indicated by the black dotted T. A unique feature in SALAD cycles was revealed as follows: after the completion of a purge for a H_2O pulse, an intermediate evacuation step was inserted, before a SPU duration was initiated, by stopping the flow of the Argon purge gas that created a laminar flow with a direction perpendicular to the surface normal of the substrate. The laminar flow established for ALD was found to create an impenetrable barrier that stopped Cu species generated in SPU from reaching the substrate. In this inaugural experiment, the SPU window was chosen after a full ALD cycle due to its simplicity that avoided an interruption of an ALD cycle.

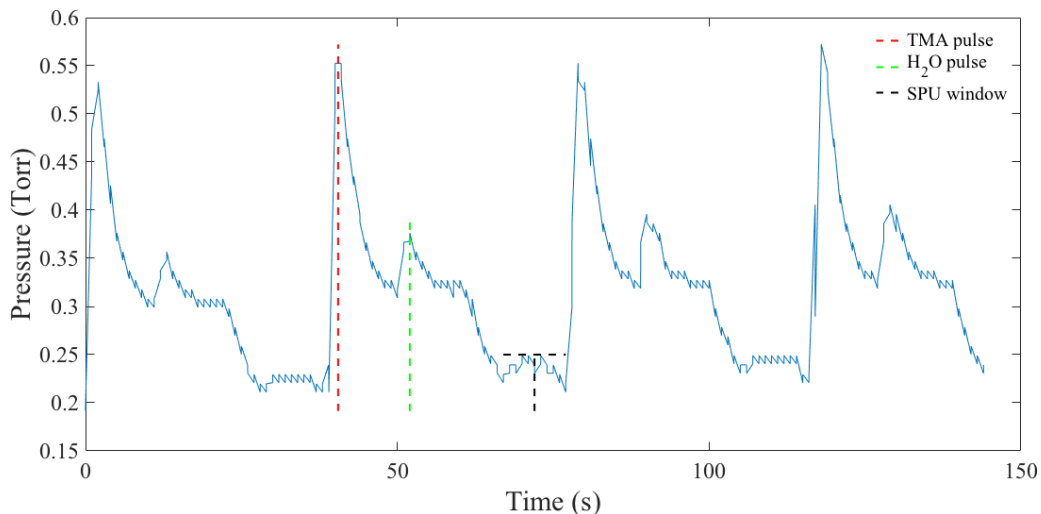


Fig. 4: Time-progressive change in the background pressure in the *SALAD* system showing a four *SALAD* cycles sampled during the preparation of the $\text{AlO}_x\text{-Cu}$ nanocomposite. Each *SALAD* cycle comprises: a TMA pulse denoted by the red dotted vertical line, a purge for TMA, a H_2O pulse denoted by the green dotted vertical line, a purge for H_2O , and a SPU duration indicated by the black dotted T.

Fig. 5 shows R collected from the samples prepared by the *SALAD* system. The R measurements were carried out to elucidate unique optical properties that would emerge from complex materials synthesized by our new deposition method *SALAD*. Two reference samples – 200 nm thick Cu film deposited by SPU only and 40 nm thick AlO_x film deposited by ALD only show R dispersions generally expected for bulk forms of pure Cu and amorphous Al_2O_3 . The R dispersion for a control Si wafer is also shown as a reference. One would expect R dispersion of the $\text{AlO}_x\text{-Cu}$ nanocomposite to somehow reflect the characteristics of R of the two constituent materials – Cu and AlO_x ; however, the $\text{AlO}_x\text{-Cu}$ nanocomposite appears to exhibit R significantly lower than that of the Cu film in the spectrum range above 550 nm where the Cu film shows R

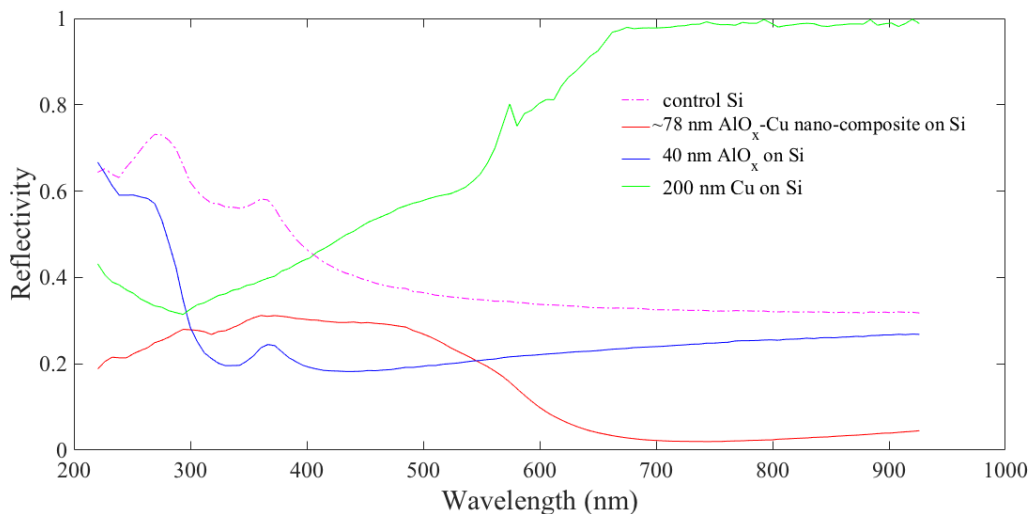


Fig. 5: Spectroscopic reflectivity obtained for samples prepared by the *SALAD* system. R was collected for the control Si wafer denoted by the pink dotted-dashed line, Si wafer coated with 40nm of *SALAD* AlO_x denoted by the solid blue curve, Si wafer coated with 200 nm of *SALAD* Cu denoted by the solid green curve, and Si wafer coated with ~78 nm of the $\text{AlO}_x\text{-Cu}$ nanocomposite.

> 0.95, which results in the $\text{AlO}_x\text{-Cu}$ nanocomposite having R dispersion that is featureless and relatively low over the visible and near-infrared spectrum region. Since the optical thickness of each of AlO_x and Cu layers in the $\text{AlO}_x\text{-Cu}$ nanocomposite is much smaller than a quarter of the wavelengths of the light used in the R measurement, destructive and constructive interferences by which conventional distributed Bragg reflectors and band-pass filters operate are not relevant in explaining unique R dispersion collected on the $\text{AlO}_x\text{-Cu}$ nanocomposite, which might suggest the presence of unique electronic interaction between multiples of AlO_x and Cu layers arranged in the $\text{AlO}_x\text{-Cu}$ nanocomposite by SALAD. Conventional nanocomposites A_yB_{1-y} made of a dielectric host made of A element that contains metal inclusions made of B element often show complex optical characteristics (e.g., significant change in R) when the dielectric-metal compositional ratio y is in the range of 0.2 - 0.8¹¹. In contrast, the $\text{AlO}_x\text{-Cu}$ nanocomposite made by SALAD shows feature-less R dispersion. Therefore, conventional effective medium theories¹² used for describing optical properties of nanocomposites do not seem to simply apply to the unique R dispersion seen on the $\text{AlO}_x\text{-Cu}$ nanocomposite. Further assessment is currently in progress to understand the unique R dispersion considering structural complexities introduced to the $\text{AlO}_x\text{-Cu}$ nanocomposite by SALAD.

5. Summary

Our unique vision of creating a deposition system capable of delivering exotic materials has been realized by demonstrating SALAD that has yielded an $\text{AlO}_x\text{-Cu}$ nanocomposite with optical properties that could not be simply assessed by knowing those of its constituent materials – ALD AlO_x and SPU Cu. A key to engineering SALAD was the modeling of gas flow in the chamber; our CFD-FEA allowed us to optimize chamber design parameters such as FASD width, chamber width, and SPU throw distance. We have demonstrated that the sequential deposition of ALD and SPU in a single chamber opening a new frontier of materials science exploration. We are confident that the extreme level of control over deposition rate and the enhanced ability to deliver a variety of chemical elements is producing materials with structural complexities that lead to novel physical phenomena.

¹ A. J. Elliot, G. A. Malek, R. Lu, S. Han, H. Yu, S. Zhao, J. Z. Wu, "Integrating atomic layer deposition and ultra-high vacuum physical vapor deposition for in situ fabrication of tunnel junctions," *Review of Scientific Instruments* 85, 073904 (2014).

² R. Ravindran, K. Gangopadhyay, S. Gangopadhyay, "Permittivity enhancement of aluminum oxide thin films with the addition of silver nanoparticles," *Applied Physics Letters* 89, 263511 (2006).

³ M. Gorbunova, L. Lemkina, I. I. Lebedeva, D. Kisel'kov, L. Chekanova, "Synthesis and potential applications of silver—porous aluminium oxide nanocomposites as prospective antiseptics and bactericides," *Journal of Materials Science: Materials in Medicine* 28, 40 (2017).

⁴ L. Maya, W. R. Allen, A. L. Glover, J. C. Mabon, "Gold nanocomposites," *Journal of Vacuum Science & Technology B* 13, 361 (1995).

⁵ N. M. Figueiredo, N. J. M. Carvalho, A. Cavaleiro, "An XPS study of Au alloyed Al-O sputtered coatings," *Applied Surface Science* 257, 5793 (2011).

⁶ V. Lozovski, M. Razumova, "Influence of inclusion shape on light absorption in thin Au/Teflon nanocomposite films," *Journal of the Optical Society of America B* 33, 8 (2016).

⁷ N. M. Figueiredo, T. Kubart, J. A. Sanchez-Garcia, R. Escobar Galindo, A. Climent-Font, A. Cavaleiro, "Optical properties and refractive index sensitivity of reactive sputtered oxide coatings with embedded Au clusters," *Journal of Applied Physics* 115, 063512 (2014).

⁸ T. Kazimierczuk, D. Fröhlich, S. Scheel, H. Stolz, M. Bayer, "Giant Rydberg excitations in the copper oxide Cu_2O ," *Nature* 514, 343 (2014).

⁹ J. Ghijsen, L. H. Tjeng, J. van Elp, H. Eskes, J. Westerink, G. A. Sawatzky, M. T. Czyzyk, "Electronic structure of Cu_2O and CuO ," *Physical Review B* 38, 11322 (1988).

¹⁰ B. K. Meyer, A. Polity, D. Reppin, M. Becker, P. Hering, P. J. Klar, T. Sander, C. Reindl, J. Benz, M. Eickhoff, C. Heiliger, M. Heinemann, J. Blasing, A. Krost, S. Shokovets, C. Müller, C. Ronning, "Binary copper oxide semiconductors: From materials towards devices," *Physica Status Solidi B* 249, 1487 (2012).

¹¹ R. W. Cohen, G. D. Cody, M. D. Coutts, B. Abeles, "Optical properties of granular silver and gold films," *Physical Review B* 8, 3689 (1973).

¹² M. Y. Koledintseva, R. E. DuBroff, R. W. Schwarts, "A Maxwell Garnett model for dielectric mixtures containing conducting particles at optical frequencies," Progress In Electromagnetics Research, PIER 63, 112 (2006).